Aliev *et al. Nanoscale Research Letters* 2012, **7**:378
http://www.nanoscalereslett.com/content/7/1/378

Nanoscale Research Letters
a SpringerOpen Journal

NANO EXPRESS Open Access

Porous silicon bulk acoustic wave resonator with integrated transducer

Gazi N Aliev[1*], Bernhard Goller[1,4], Paul A Snow[1], Helge Heinrich[2], Biao Yuan[2] and Robert Aigner[3]

Abstract

We report that porous silicon acoustic Bragg reflectors and AlN-based transducers can be successfully combined and processed in a commercial solidly mounted resonator production line. The resulting device takes advantage of the unique acoustic properties of porous silicon in order to form a monolithically integrated bulk acoustic wave resonator.

Keywords: Porous silicon, Acoustic resonator, BAW filter, Acoustic Bragg mirror

Background

In 1982, Lakin et al.[1] demonstrated the potential for thin-film bulk acoustic wave (BAW) devices for filters and resonators. Acoustic filters such as surface acoustic wave (SAW) filters and BAW filters are a cornerstone of modern wireless communication as they enable radio frequency (RF) filters with very low loss, excellent frequency selectivity and very small size. The frequency spectrum in the range between 400 MHz and 3 GHz is packed with bands allocated to various broadcasting and wireless communication systems. Avoiding interference between various systems is becoming increasingly difficult. Effective use of this spectrum requires RF filters to meet demanding specifications with regard to steepness of the transition between passband and adjacent rejection bands. The market for RF filters has grown to more than 3 billion units per year, while unit price is in a steady decline and averaged less than $0.25 in 2011. BAW filters are used for the most demanding applications - as they outperform SAW filters - but they require a complex manufacturing process which is more expensive. In BAW devices, the acoustic wave, generated in a thin-film piezoelectric layer sandwiched between electrodes, propagates in a vertical direction towards the substrate. The frequency of the acoustic resonance is determined by the thickness of the piezolayer and the mass of the electrodes but must be confined by structuring the substrate. In a film bulk acoustic resonator (FBAR), a cavity is etched below the active structure to create a suspended membrane. Alternatively, an acoustic distributed Bragg reflector (ADBR) can be used to stop the acoustic wave penetrating the substrate. These devices are called solidly mounted resonators (SMR). SMR-BAW devices have the advantages over FBAR structures that they are less delicate to manufacture, more rugged when produced and have better power handling as they have thermal contact with the substrate[2,3]. A schematic cross-section of an SMR is shown in Figure 1.

For commercial acoustic mirrors which are components of SMRs and filters, a low-acoustic impedance material such as SiO_2 is layered with high-impedance materials such as tungsten or molybdenum [2]. Recently, it has been suggested that metal-oxide ADBRs could be replaced by porous silicon (PSi) ADBR [4]. This has several advantages: the potential for integrated devices on a Si substrate, the elimination of several processing steps, the impedance mismatch (defining the bandwidth) can be easily and continuously adjusted, advanced filter design including apodization, impedance matching and rugatization become possible [5], and no lattice mismatch exist between the layers of the ADBR; thus, the interfaces are smoother leading to lower losses and better device performance.

For an ADBR, the center frequency of stop bands f_B for different orders m, for normal incidence of the wave, can be expressed as:

$$f_B = (m/2)\,(d_1/v_1 + d_2/v_2)^{-1},\ m = 1, 2, 3, \ldots, \qquad (1)$$

where d_i and v_i are the thickness and the acoustic velocity of the two alternating layers, respectively. The

*Correspondence: g.aliev@bath.ac.uk
[1] Department of Physics, University of Bath, Claverton Down, Bath, BA2 7AY, UK
Full list of author information is available at the end of the article

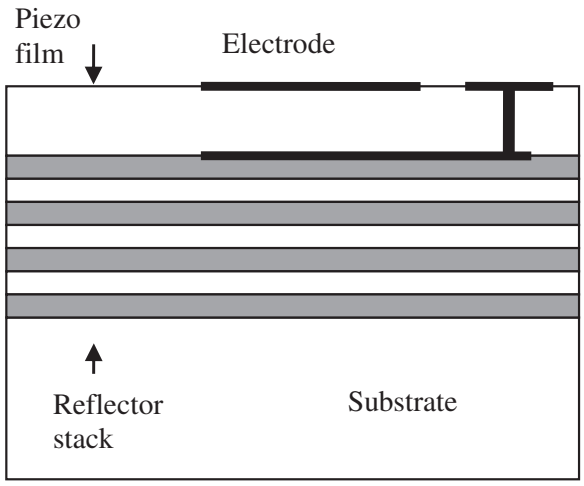

Figure 1 Schematic cross-section of solidly mounted resonator (SMR). A piezo resonator is sandwiched between two electrodes and mounted on an acoustic Bragg reflector.

corresponding gap widths Δf^b for odd and Δf^c for even m can be expressed following reference [6] as:

$$\Delta f^b = (4 f_B/\pi m)\left|M\cos(2\pi f_B \zeta)\right|,\ m = 1,3,5,\ldots$$

$$\Delta f^c = (4 f_B/\pi m)\left|M\sin(2\pi f_B \zeta)\right|,\ m = 2,4,6,\ldots, \quad (2)$$

where $M = (\rho_1 v_1 - \rho_2 v_2)/(\rho_1 v_1 + \rho_2 v_2)$, $\zeta = d_1/v_1 - d_2/v_2$, and ρ_i is the mass density of the layers. It can be seen that the gap width depends on M which is the acoustic impedance mismatch between the layers and on ζ which is the difference in the time required for an acoustic wave to cross the layers in the structure. When $d_1/v_1 = d_2/v_2$, as follows from Equations 1 and 2, all gaps with even m disappear, and widths of all gaps with odd m become equal.

Mass density ρ and acoustic velocity v in PSi are functions of porosity, i.e., the volume fraction of voids ϕ and can be expressed as $\rho = \rho_0(1-\phi)$ and $v = v_0(1-\phi)^\kappa$, where ρ_0 and v_0 are mass density and acoustic velocity of bulk Si, respectively, and κ is a parameter which depends on PSi morphology. To design ADBRs, the results of the recently published comprehensive study of porosity dependence of acoustic velocity in PSi[7] have been used. For the type of a Si wafer used in this work, $\kappa = 0.77$.

Here, we demonstrate that AlN transducer can be successfully integrated, in a commercial BAW-SMR production line, with an electrochemically etched PSi acoustic mirror consisting of a single layer or a multilayered stack. We present results on individual devices defined on a Si wafer by lithography.

Methods

PSi ADBRs and single layers were fabricated using electrochemical etching[8]. The wafer material used was highly-boron-doped CZ silicon with maximum resistivity of 25 mΩcm, with 150-mm diameter and 675±20-μm thickness. Room temperature anodization was performed in a 1:1 solution of 49% aqueous HF and hydrous ethanol. High- and low-porosity layers were obtained by alternating the current density (50 to 150 mA/cm^2). The thickness of the layers was controlled by the etch duration. Subareas of a wafer, of diameter 40 mm, were etched separately

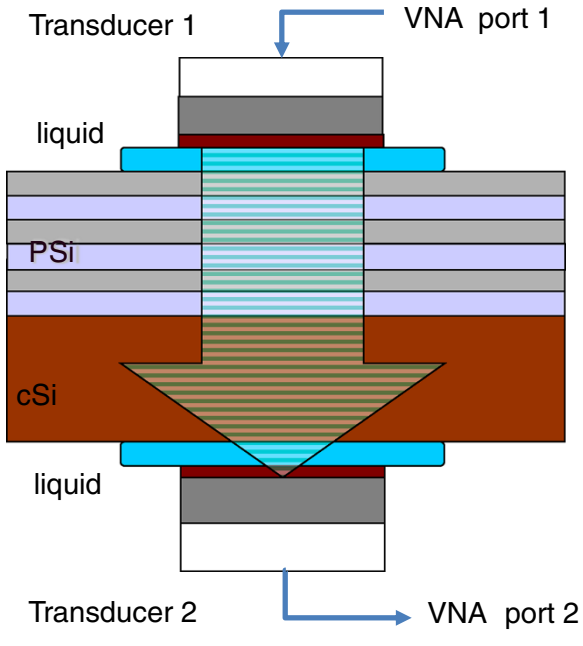

Figure 2 Schematic of experimental setup used for acoustic transmission measurement. cSi, bulk crystalline Si.

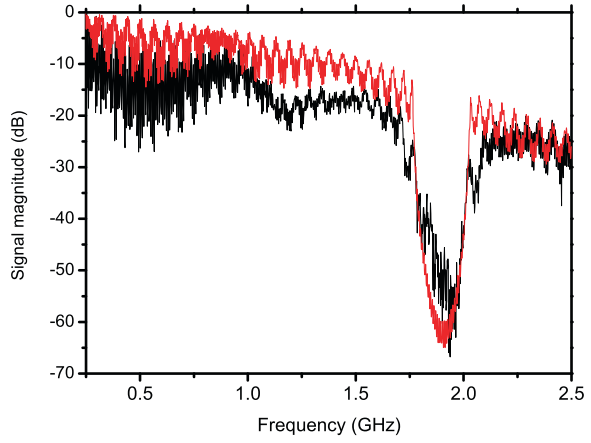

Figure 3 Acoustic transmission spectrum. Black line, measured acoustic wave transmission spectrum through a PSi ADBR on a bulk Si substrate. The transmission, recorded on a semi-logarithmic scale, is corrected by the envelope function of the transducers response. Red line, calculated spectrum.

Table 1 Thickness and composition of deposited layers

Function	Material	Nominal thickness (nm)	Impedance (MRayl)	Longitudinal velocity (ms^{-1})
Top electrode	AlCu	130	17	6,420
	W	120	101	5,230
Piezo layer	AlN	1300	37	10,400
Bottom electrode	W	170	101	5,230
	AlCu	200	17	6,420
Coupling layer	SiO_2	500	13	5,970
Seal to PSi	Amorphous Si	20	20	8,400
Porous layer/multilayers	PSi	variable	variable	variable

to allow investigation of different PSi structures. A set of single-layer mirrors of thickness of λ at 1.9 GHz was etched with porosity from 30% to 75%. Also, a set of ADBRs was etched with the number of repeats of the alternating layers varying from 5 to 30. The full analysis of these characterization results will be presented elsewhere.

To characterize the etched ADBR, the acoustic transmission spectrum was measured using the experimental technique shown schematically in Figure 2. A specimen was placed between two external transducers operating with a central frequency at 1 GHz. Each transducer consists of a ZnO piezoelectric layer driving waves into a square silicon pillar 160 $\mu m \times 160\ \mu m \times 500\ \mu m$ with a thin (few microns) SiO_2 antireflection coat. Transducers were coupled to the specimen via water or In-Ga eutectic. Acoustic waves were emitted normally into the PSi layers with uncertainty in alignment of less than 0.5°. Under these conditions, no shear waves were excited in the PSi. The transducers were connected to two ports of a vector network analyzer (VNA), and the signal transmitted through structure was measured as an S_{21}-parameter with sweeps performed from 0.2 to 2.5 GHz with a bandwidth of 100 Hz and a resolution of 0.75 MHz. Scattering parameters (*S*-parameters) are determined by measuring the magnitude and phase of the incident, transmitted and reflected voltage signals[9]: $S_{11} = \frac{reflected}{incident}$, $S_{21} = \frac{transmitted}{incident}$.

The spectrum has been modelled using a generalized matrix method given by Mitsas and Siapkas [10] for optical wave propagation through multilayered structure. The method is convenient to include wave scattering on interface roughness. At normal incidence for acoustic waves, this method can be used for both optical and acoustic waves by replacing optical admittance, i.e., refractive index n with the acoustic admittance $1/Z$, where $Z = \rho v$. The BAW device actuator layers were deposited in commercial BAW production line using fully automated production equipment and process control (TriQuint Semiconductor, 1818 S HW441, Apopka, FL, 32703, USA). The thicknesses were monitored by laser-acoustic measurements, optical interferometry and precision mass metrology.

Layer thicknesses for the processed PSi layers were obtained from TEM measurements on sample devices. A map of oxygen concentration for a device has been obtained from energy-filtered TEM microscopy.

The final BAW-SMR devices were tested by RF-probing for a 1-port *S*-parameter (S_{11}) measurement of the electrical impedance with sweeps performed from 0.2 to 4.2 GHz with a resolution of 0.5 MHz.

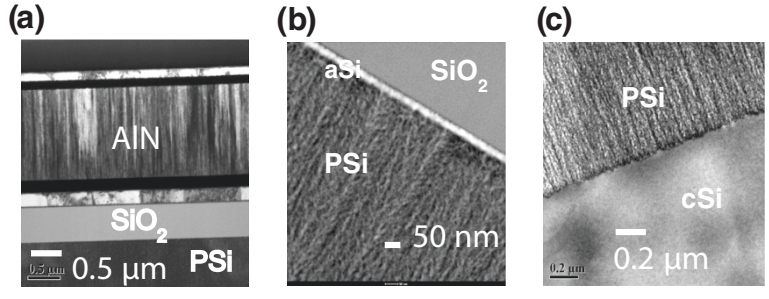

Figure 4 TEM cross-sections. (**a**) The BAW actuator stack showing the metallic layers of the electrodes and the coupling layer of SiO_2 above a PSi single layer. (**b**) The interface between an etched PSi single layer and the SiO_2 coupling layer. The amorphous Si layer was used to seal the PSi layer to avoid any contamination of the production line. (**c**) Typical interface between PSi and cSi. Scale bars are shown in each micrograph.

Results and discussion

Acoustic distributed Bragg reflector: acoustic transmittance measurement with simulation

Figure 3 (black line) shows the acoustic transmission band gap measured for the PSi ADBR consisting of 30 pairs of layers on the Si substrate with an unpolished backside, before deposition of the actuator stack. Layers in the ADBR were designed to form halfwave-thick pairs of layers for the 1.9-GHz longitudinal acoustic waves aiming for 200-MHz gap width. The layer porosity was 45% and 51% with layer thicknesses of 0.71 μm and 0.65 μm for the alternating layers of PSi, respectively. The porosity and thicknesses of the layers were chosen to place the stop bands within the bandwidth of the AlN transducer to be deposited on the top of the ADBR. The fine features of the spectrum are not noise but the longitudinal modes of the Si pillars of the transducers and the Si substrate of the sample. The result of modelling all the layers in the system, including transducers, fluid and substrate, is shown in Figure 3 by the red line. Good agreement between modelled and measured spectra is seen. The low frequency bumps are acoustic modes from the coupling liquid used. There is some discrepancy between theory and experiment in the region of about 1.2 GHz, which comes from the correction procedure for aggregate response from both transducers near the emission peak for a single transducer. The experimental coupling of the acoustic waves between transducers slightly varies from that of the idealized model of travelling plane waves.

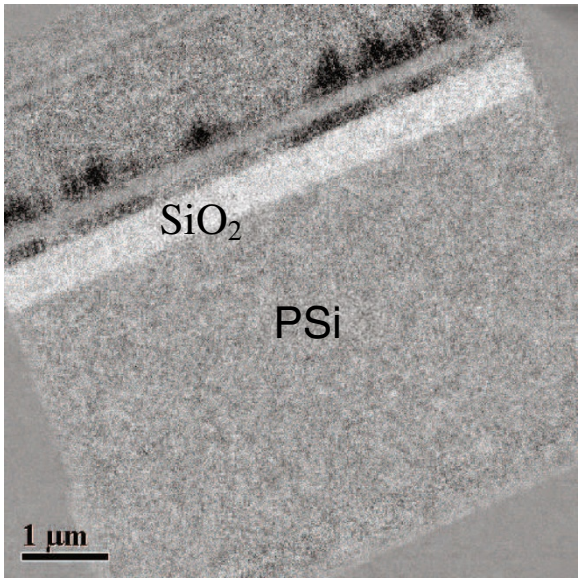

Figure 5 Map of oxygen concentration. The distribution of oxygen across the layers shows a good interface between the deposited SiO_2 and the PSi. There is no oxygen gradient apparent through the PSi layer.

BAW resonator: design and fabrication

The transducers were deposited with the layers, materials and thicknesses shown in Table 1. The thicknesses aim at an operating frequency of 1.9 GHz. The surface of a PSi single layer or an ADBR was sealed by 20 nm of reactively RF magnetron sputtered amorphous Si (aSi) and coupled to the transducer via a 0.5-μm SiO_2 layer. This aSi layer was used to mitigate the risk of contamination for subsequent processes. The bottom electrode is unpatterned and grounded by capacitive coupling to a ground plane formed by metal layer covering the entire periphery of the resonator. The top electrode defines the driven resonator and has an area of 2.35×10^4 μm^2. A 1.3-μm AlN piezo layer was sandwiched between AlCu/W electrodes. In order to achieve a highly piezoelectric AlN films, the bottom electrode must exhibit uniform grain orientation and near atomic smoothness. The AlN layer was deposited using reactive sputtering in DC-pulsed mode from a pure Al target in nitrogen and argon plasma. Stress control in AlN is achieved using additional RF bias applied to the wafer chuck. Both the AlCu and W layers were deposited by DC-pulsed sputtering. The top electrode layer was patterned and etched with reactive ion etching in a high-density plasma reactor.

Figure 4a shows a micrograph of a deposited transducer. It can be seen that the SiO_2 layer has a clean interface with the PSi. Figure 4b,c shows examples of interfaces of PSi with a top interface with deposited aSi cap and the unetched substrate layers. The typical directional mesopores of PSi etched from highly p-doped material are clear with a slight roughness at the PSi/Si-substrate interface. The acoustic wavelength is $\sim$ 3 μm, so the roughness is approximately on the scale of 1% of the wavelength and, therefore, not a significant source of loss from interface roughness scattering. The backside of the wafer was polished to a nearly optical mirror surface finish to reduce scattering at that surface.

Figure 5 shows a map of oxygen concentration for a device obtained from energy-filtered TEM microscopy. It is clear that there is a consistent oxygen level across the PSi layer with no gradients apparent after processing. However, this does suggest that some oxidation of the PSi has occurred.

Figure 6 shows typical raw data of the S_{11} response (i.e., reflection) for SMR structure with an integrated transducer (see schematic in Figure 7). The ADBR used for this particular example was of identical design to that demonstrated in Figure 3. The spectrum in green shows data from a device located over an unetched part of the Si wafer. This is, thus, the AlN transducer response coupled into the Si substrate. The fine features are the acoustic modes of the substrate. As can be seen from Figure 6 (black line), for the device with the ADBR below the transducer, the modes from the substrate have almost

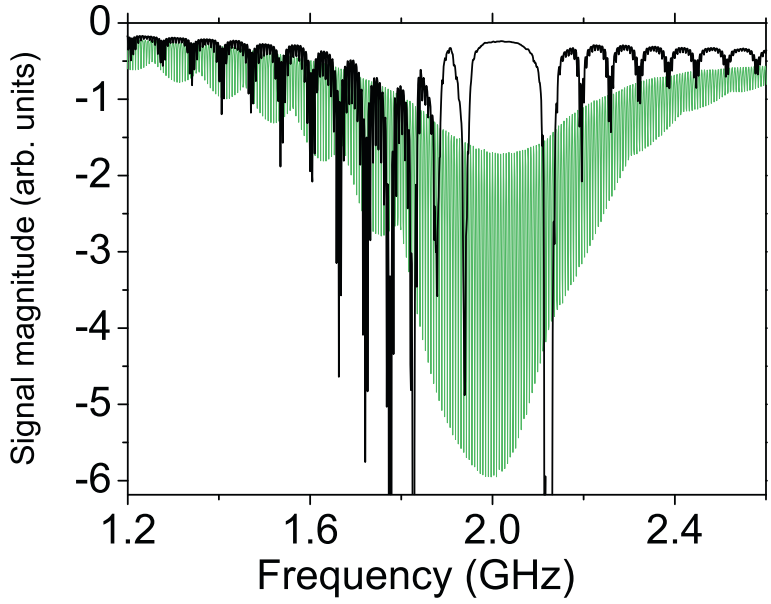

Figure 6 Measured RF S_{11} spectrum. Green line, the signal magnitude measured on a device on the processed wafer where the BAW actuator stack was deposited onto the bulk Si substrate. The fine features are acoustic modes from the substrate. Black line, signal magnitude measured on a device where the BAW actuator stack was deposited above a PSi ADBR with 30 pairs of layers.

completely disappeared. Only the modes from the Bragg reflector are seen. The position of the acoustic gap in Figure 6 is slightly shifted to higher frequencies compared with the gap position in Figure 3; however, the gap width is the same. The small shift of the acoustic gap is not fully understood at the moment. A slight change in the etching conditions during PSi ADBR fabrication, such as wafer doping level or etchant temperature, can change porosity or layer thickness. The effect of layer oxidation during the processing steps in the production line can also shift the stop band due to possible changes to porosity, acoustic velocity and thickness of the layers. When understood, these effects can be mitigated against by better control of production conditions and allowance for the change in material properties during processing.

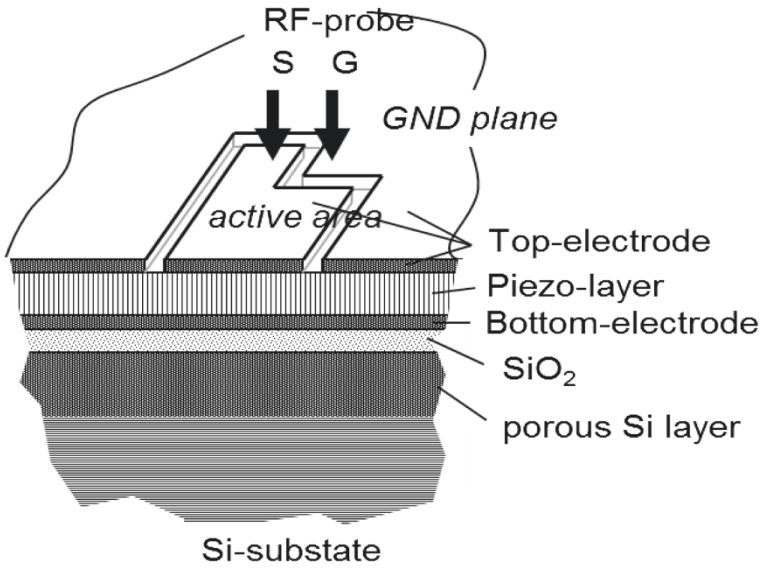

Figure 7 Whole device under the test.

Conclusions

We have demonstrated that porous silicon processing can be successfully combined with thin-film deposition methods needed to create high-performance BAW resonators. Adjustment of acoustic properties by changing a single process parameter is a unique feature of porous silicon and highly attractive for future BAW devices.

Competing interests
The authors declare that they have no competing interests.

Acknowledgements
This work was partly supported by the Engineering and Physical Sciences Research Council (UK) under grant EP/J007552/1. Financial support for TEM measurements was provided in part by the Florida High Tech Corridor Industry Matching Research Program of the University of Florida.

Author details
[1]Department of Physics, University of Bath, Claverton Down, Bath, BA2 7AY, UK. [2]Advanced Materials Processing and Analysis Center (AMPAC), University of Central Florida, 4000 Central Florida Blvd., Orlando, FL, 32816-2455, USA. [3]TriQuint Semiconductor, 1818 S HW441, Apopka, FL, 32703, USA. [4]Infineon Technologies AG, Siemensstrasse 2, Villach, 9500, Austria.

Authors' contributions
GNA proposed PSi-based BAW SMR device fabrication, designed ADBR structures and contributed to their fabrication, carried out acoustic transmission measurements with data analysis and simulation, and drafted the manuscript; BG fabricated ADBR structures and contributed to acoustic transmission measurements, data analysis and drafting; PAS proposed PSi-based BAW SMR device fabrication and contributed to data analysis and drafting; HH and BY carried out TEM and EFTEM measurements; RA designed and managed fabrication of BAW SMR devices, carried out RF measurements with data analysis and simulation, and contributed to drafting. All authors read and approved the final manuscript.

Received: 30 April 2012 Accepted: 9 July 2012
Published: 9 July 2012

References

1. Lakin KM, Wang J, Kline G, Landin A, Chen Y, Hunt J: **Thin film resonators and filters.** *Proc IEEE Ultrasonics Symp* 1982, **1:**466–475.
2. Satoh Y, Nishihara T, Yokoyama T, Ueda M, Miyashita T: **Development of piezoelectric thin film resonator and its impact on future wireless communication systems.** *Jpn J Appl Phys* 2005, **44:**2883–2894.
3. Mahon S, Aigner R: **Bulk acoustic wave devices – why, how, and where they are going.** In *CS MANTECH Conference: May 14-17 2007; Austin, Texas, USA*. Edited by Compound Semiconductor Manufacturing Technology Organization: CS MANTECH; 2007:15–18.
4. Aliev GN, Goller B, Kovalev D, Snow PA: **Hypersonic acoustic mirrors and microcavities in porous silicon.** *Appl Phys Lett* 2010, **96:**124101.
5. Lorenzo E, Oton CJ, Capuj NE, Ghulinyan M, Navarro-Urrios D, Gaburro Z, Pavesi L: **Porous silicon-based rugate filters.** *Appl Opt* 2005, **44:**5415–5421.
6. Santos PV, Ley L, Mebert J, Koblinger O: **Frequency gaps for acoustic phonons in α-Si:H/α-SiN_x:H superlattices.** *Phys Rev B* 1987, **36:**4858–4867.
7. Aliev GN, Goller B, Snow PA: **Elastic properties of porous silicon studied by acoustic transmission spectroscopy.** *J Appl Phys* 2011, **110:**043534.
8. Lehmann V: *Electrochemistry of Silicon*. Weinheim: Wiley-VCH; 2002.
9. Agilent Technologies Inc.: **Agilent network analyzer basics.** [http://cp.literature.agilent.com/litweb/pdf/5965-7917E.pdf].
10. Mitsas CL, Siapkas DI: **Generalized matrix method for analysis of coherent and incoherent reflectance and transmittance of multilayer structures with rough surfaces, interfaces, and finite substrates.** *Appl Opt* 1995, **34:**1678–1683.

doi:10.1186/1556-276X-7-378
Cite this article as: Aliev *et al.*: Porous silicon bulk acoustic wave resonator with integrated transducer. *Nanoscale Research Letters* 2012 **7**:378.